ANALYTIC MIXED VARIATIONAL BEAM APPROACH FOR THIN-WALLED COMPOSITE BLADES WITH THREE-DIMENSIONAL WARPINGS

Jae Seong Bae, Konkuk University, Seoul 05029, Republic of Korea
Sung Nam Jung, Konkuk University, Seoul 05029, Republic of Korea

Abstract

A variationally consistent, analytical linear beam theory that describes the model in a Timoshenko-Vlasov level is developed using the foundation of the Reissner's mixed variational theorem. Formulated based on the shell theory, all the field governing equations (equilibrium and continuity) and the boundary conditions of the shell wall as well as the stiffness constants of the beam are derived in closed form. In the beam constitutive relations, no peculiar or ad hoc assumptions are introduced to simplify the analysis. The mixed method enables to obtain the reactive stresses and sectional warpings (both in- and out-of-plane) which are evaluated through a progressive step, depending on the level of the beam approximations. The stress recovery capability is incorporated in the post stage of the analysis to compute the sectional stresses distributed over the beam cross-section. The current analysis is validated on sectional warpings, stiffnesses, and stresses for several benchmark examples available in the literature. The comparison study demonstrates good agreements with detailed three-dimensional (3D) finite element (FE) analysis and state-of-the-art beam analysis results. The influence of including the in-plane warpings is shown to be marginal on stiffness constants of a thin-walled box beam, with slightly improved predictions.

1. NOTATION[1]

Symbols

a	Local shell radius of curvature
F_x	Axial force along x axis
F_y, F_z	Shear forces along y and z axes
M_x	Torsional moment about x axis
M_y, M_z	Bending moments about y and z axes
M_ω	Torsional bi-moment
M_{xx}, M_{ss}, M_{xs}	Bending and twisting couples of the shell wall
N_{xx}, N_{ss}, N_{xs}	In-plane stress resultants of the shell wall
N_{xn}, N_{sn}	Transverse shear stress resultants of the shell wall
U, V, W	Translational displacements of beam sectional reference origin along x, y, z axes
u, v, w	Translational displacements of an arbitrary material point of beam section along x, y, z axes
u_x, u_s, u_n	Translational displacements of the shell wall along x, s, n axes
β_y, β_z	Sectional rotation angles about y and z axes
γ_{xn}, γ_{sn}	Transverse shear strains of the shell wall
γ_{xy}, γ_{xz}	Transverse shear strains of the beam in x-y, x-z plane
γ_{xs}	In-plane shear strain of the shell wall
$\epsilon_{xx}, \epsilon_{ss}$	In-plane normal strains of the shell wall
$\kappa_{xx}, \kappa_{ss}, \kappa_{xs}$	Curvatures of the shell wall
ϕ	Sectional rotation angle about x axis
ψ_x, ψ_s	Rotation angles of the shell wall about s, x axis
$\omega_x, \omega_y, \omega_z$	Contour warping functions along x, y, z axis

Subscripts

$()_{,x}, ()_{,s}$	$\partial()/\partial x, \partial()/\partial s$

Superscripts

$()^{\mathrm{T}}$	Transpose of an array
$()^{-1}$	Inversion of an array

2. INTRODUCTION

Thin-walled beams made of advanced composites exhibit complex mechanical behavior that cannot be observed for conventional isotropic counterpart structures. Particularly, anisotropic composites induce elastic couplings between various deformation modes such as extension, bending, torsion, and shear, which makes the analysis more involved. It is conceived that three-dimensional (3D) solid or shell finite element (FE) approaches lead to solutions of high resolution, however, these numerical methods essentially demand heavy computational costs with large modeling effort. In this context, development of efficient and accurate analysis methodologies for thin-walled composite beams has been a key research topic in the fields of the static and dynamic analyses of helicopter and wind turbine blades (Refs. 1-4).

The theoretical foundation for the modern composite beam analysis has been established by Berdichevskii (Ref. 5) who justifies the decomposition of the 3D elasticity theory of the structure into 1D global beam problem and 2D local cross-section analysis, using the variational asymptotic arguments (Ref. 2). While the original 3D nature of the beam is essentially represented with the cross-sectional stiffness constants, a correct treatment of the sectional warpings is crucial for the successful development of a beam model. Many generic beam theories have been devised considering detailed cross-sectional warpings and elastic coupling effects of composites. These range from FE-based cross-sectional analyses (Refs. 6-9), polynomial or series expansion methods (Refs. 10-12), closed-form elasticity solutions (Ref. 13), contour-based analytic formulations (Refs. 14-19), and to semi-analytic approaches (Refs. 20-22).

Each method has its own pros and cons depending upon kinematic foundations and numerical schemes adopted in the solution schemes. Among these the closed-form analytical method has clear benefits in terms of computational efficiency and modeling simplicity. In addition, no serious discretization on 2D cross-sectional domain is needed which is typical in FE-based approach. Instead, the thin-walled profile of a beam section is modeled as an assembly of 1D line segments which enables to compute the cross-sectional constants with simple analytic integrals. Although degeneration of the cross-sectional information is inevitable, the beam response can be obtained in a set of closed-form solutions where the influences of beam sectional parameters can clearly be visible. Most of the analytical formulations have been founded based on simplifying (*ad hoc*) assumptions such as the sectional rigidity in its own plane (Refs. 1-2).

There exist several analytical approaches in which none or the least level of beam assumptions are introduced. Hodges and his coworkers (Refs. 23-25) applied the variational-asymptotic method (VAM) to evaluate the stiffness constants and 3D warpings for anisotropic beams. In this method, the characteristic dimensions of the cross-section are assumed small as compared with the wavelength of the beam deformation to find the desired representation of the beam model. The theory is straightforward and rigorous in mathematical terms, capturing 3D warpings and elastic coupling effects precisely. However, an iterative asymptotic expansion is needed to systematically eliminate higher-order terms from the energy expression. Furthermore, there is a difficulty in reaching a Timoshenko-Vlasov level beam that takes into account the effects of the transverse shear and warping restraint simultaneously. Reissner and Tsai (Ref. 26) presented generalized solution procedures starting from the linear shell theory to obtain the sectional stiffness constants and 3D contour warpings for anisotropic beams under extension, torsion, and bending. Tsai (Ref. 27) extended this concept to determine the exact expressions for shell stress resultants and 3D warpings under the action of pure shear loads. Though the method is generic and mathematically sound, the application is limited to simple cross-sections with homogeneity. Jung et al. (Ref. 15) derived the beam stiffness constants based on the Reissner's mixed variational principle (Ref. 28). Even though a simplifying assumption is adopted, with some limitations in the beam formulation, the shell stress resultants obtained from the mixed principle led to accurate analysis results for coupled composite beams with inhomogeneity.

In the present work, a variationally consistent, analytical beam formulation that represents the beam in a Timoshenko-Vlasov level is developed based on the foundation of Reissner’s mixed variational theorem (Ref. 13). With the shell theory as the starting point, all the field governing equations (equilibrium and continuity) as well as boundary conditions of the shell wall leading to (7×7) stiffness coefficients are derived in closed form. Unlike most of the existing engineering beam theories, no priori or simplifying assumptions are introduced in describing the beam formulation. The resulting section stiffness constants reflect the effect of the sectional deformations over both in- and out-of-plane directions of the beam. The stress recovery analysis is incorporated also to evaluate the layerwise distribution of stresses and strains distributed over the cross-sectional wall.

3. THEORY

3.1. Strain-displacement relations

Figure 1 shows a thin-walled beam section with reference coordinate frames. Two reference frames are used: one is for the global beam with an orthogonal Cartesian coordinate system (x, y, z) and the other is for the local shell wall with a curvilinear coordinate system (x, s, n). On each reference frame, the respective roto-translational displacements are defined with their positive directions, as shown in Fig. 1. Assuming small strains and small local rotations, the strain- and curvature-displacement relations for the shell wall can be written (Ref. 15).

$$
\begin{aligned}
&\epsilon_{xx}^0 = u_{x,x}^0; \quad \epsilon_{ss}^0 = u_{s,s}^0 + u_n^0/a; \quad \gamma_{xs}^0 = u_{x,s}^0 + u_{s,x}^0 \\
&\kappa_{xx} = \psi_{x,x}; \quad \kappa_{ss} = \psi_{s,s}; \quad \kappa_{xs} = \psi_{x,s} + \psi_{s,x} \\
&\gamma_{xn} = u_{n,x}^0 + \psi_x; \quad \gamma_{sn} = u_{n,s}^0 + \psi_x - u_s^0/a
\end{aligned} \tag{1}
$$

The shell midplane displacements (u_x^0, u_s^0, u_n^0, ψ_x, ψ_s) are expressed in terms of the beam displacements (U, V, W, ϕ, β_y, β_z) after some manipulations of the shell strains in Eq. (1) as follows (Refs. 15, 26-27):

$$
\begin{aligned}
u_x^0 &= U + z\beta_y - y\beta_z + \omega_x \\
u_s^0 &= y_{,s}V + z_{,s}W + r_n\phi + \omega_y y_{,s} + \omega_z z_{,s} \\
u_n^0 &= z_{,s}V - y_{,s}W - r_t\phi + \omega_y z_{,s} - \omega_z y_{,s} \\
\psi_x &= -y_{,s}\beta_y - z_{,s}\beta_z + r_t\phi_{,x} - \omega_{y,x}z_{,s} + \omega_{z,x}y_{,s} \\
\psi_s &= \phi + \Psi_s
\end{aligned} \tag{2}
$$

where $y_{,s} = -\sin\alpha$ and $z_{,s} = \cos\alpha$ are the direction cosines with α being the orientation angle with respect to y axis (Fig. 1), and r_n and r_t are the normal and tangential coordinates of a point on the shell midplane along n and s axis, measured from the section reference origin (Fig. 1), respectively. In Eq. (2), ω_x, ω_y and ω_z are the translational warping functions defined along the midplane contour. Ψ_s is the elastic bending angle about x axis. These terms

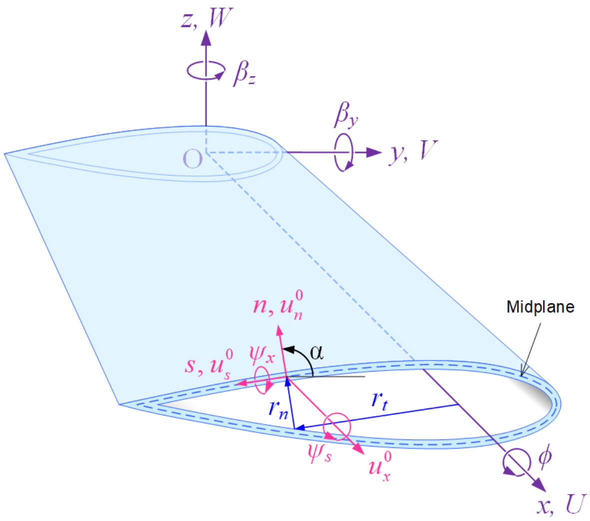

Figure 1. Schematic of the reference coordinate frames.

denote elastic deformations of the section contour whose explicit expressions are given by (Refs. 26-27):

$$
\begin{aligned}
\Psi_s &= \int_{s_0}^{s} \kappa_{ss}\,ds \\
\omega_y &= -z\Psi_s + \int_{s_0}^{s}\left(y_{,s}\epsilon_{ss}^0 + z_{,s}\gamma_{sn} + z\kappa_{ss}\right)ds \\
\omega_z &= y\Psi_s + \int_{s_0}^{s}\left(z_{,s}\epsilon_{ss}^0 - y_{,s}\gamma_{sn} - y\kappa_{ss}\right)ds \\
\omega_x &= \int_{s_0}^{s}\gamma_{xs}^0\,ds - \int_{s_0}^{s} r_n\,ds\,\phi_{,x} - \int_{s_0}^{s}\left(\omega_{y,x}y_{,s} + \omega_{z,x}z_{,s}\right)ds
\end{aligned} \tag{3}
$$

The warping functions ω_x, ω_y, ω_z, and Ψ_s are not known a priori but obtained analytically through an iterative process that will be explained later. Shell displacements in Eq. (2) can be transformed into beam displacement components as follows.

$$
\begin{aligned}
u(x,y,z) &= U(x) + z\beta_y(x) - y\beta_z(x) + \omega_x \\
v(x,y,z) &= V(x) - z\phi(x) + \omega_y \\
w(x,y,z) &= W(x) + y\phi(x) + \omega_z
\end{aligned} \tag{4}
$$

Shell strains in Eq. (1) can be expressed in terms of the beam displacements by inserting Eq. (2) into Eq. (1). Among the shell strains in Eq. (1), we treat (ϵ_{xx}^0, κ_{xx}, κ_{xs}) as the active strains which describe the fundamental behavior of pure extension, torsion and bending of a beam following the definitions in Refs. 15, 26, and 27. The active strain components in Eq. (1) can be expressed in terms of the beam displacements as

$$
\boldsymbol{\epsilon}_a = \mathbf{B}_q\mathbf{q}_e + \boldsymbol{\epsilon}_{ax} \tag{5}
$$

where

$$
\begin{aligned}
&\boldsymbol{\epsilon}_a = \begin{bmatrix} \epsilon^0_{xx} & \kappa_{xx} & \kappa_{xs} \end{bmatrix}^{\mathrm{T}} \\
&\mathbf{B}_q = \begin{bmatrix} 1 & 0 & z & -y \\ 0 & 0 & -y_{,s} & -z_{,s} \\ 0 & 2 & 0 & 0 \end{bmatrix} \\
&\mathbf{q}_e = \begin{bmatrix} U_{,x} & \phi_{,x} & \beta_{y,x} & \beta_{z,x} \end{bmatrix}^{\mathrm{T}} \\
&\boldsymbol{\epsilon}_{ax} = \begin{bmatrix} \omega_{x,x} & r_t\phi_{,xx} - \omega_{y,xx} z_{,s} + \omega_{z,xx} y_{,s} & 2\Psi_{s,x} \end{bmatrix}^{\mathrm{T}}
\end{aligned} \tag{6}
$$

where $\boldsymbol{\epsilon}_a$ is the active strain vector and $\mathbf{q}_e$ is the generalized beam strain vector, respectively. The first part of the active strains $\boldsymbol{\epsilon}_a$ denotes the axial strains under pure extension, twist and bending, and the second part represents the variations with respect to *x*.

3.2. Laminate constitutive relations

The classical lamination plate theory (Ref. 30) is used to relate the stress resultants and couples with the shell strains as follows:

$$
\begin{aligned}
&\begin{bmatrix} \mathbf{N} \\ \mathbf{M} \end{bmatrix} = \begin{bmatrix} \mathbf{A} & \mathbf{B} \\ \mathbf{B} & \mathbf{D} \end{bmatrix} \begin{bmatrix} \boldsymbol{\epsilon}^0 \\ \boldsymbol{\kappa} \end{bmatrix} \\
&\mathbf{Q} = k\mathbf{A}_\gamma \boldsymbol{\gamma}
\end{aligned} \tag{7}
$$

where

$$
\begin{aligned}
&\mathbf{N} = \begin{bmatrix} N_{xx} & N_{ss} & N_{xs} \end{bmatrix}^{\mathrm{T}}; \quad \mathbf{M} = \begin{bmatrix} M_{xx} & M_{ss} & M_{xs} \end{bmatrix}^{\mathrm{T}} \\
&\mathbf{Q} = \begin{bmatrix} N_{xn} & N_{sn} \end{bmatrix}^{\mathrm{T}}; \quad \boldsymbol{\epsilon}^0 = \begin{bmatrix} \epsilon^0_{xx} & \epsilon^0_{ss} & \gamma^0_{xs} \end{bmatrix}^{\mathrm{T}} \\
&\boldsymbol{\kappa} = \begin{bmatrix} \kappa_{xx} & \kappa_{ss} & \kappa_{xs} \end{bmatrix}^{\mathrm{T}}; \quad \boldsymbol{\gamma} = \begin{bmatrix} \gamma_{xn} & \gamma_{sn} \end{bmatrix}^{\mathrm{T}}
\end{aligned} \tag{8}
$$

where $\mathbf{N}$, $\mathbf{M}$, $\mathbf{Q}$ are the stress resultants and couples of the laminate and $\mathbf{A}$, $\mathbf{B}$, $\mathbf{D}$, and $\mathbf{A}_\gamma$ are the laminate stiffness matrices for the extension, extension-bending coupling, bending, and shear (Ref. 30), respectively, and k (=5/6) is the shear correction coefficient. While shifting the reactive components of shell stress resultants and couples such as (N_{xs}, M_{ss}, N_{ss}, N_{sn}) into the right-hand side of the equation, one can express the shell constitutive relations in a semi-inverted form as (Refs. 15, 26-27):

$$
\begin{bmatrix} \mathbf{p}_r \\ \boldsymbol{\epsilon}_r \end{bmatrix} = \begin{bmatrix} \mathbf{C}_{aa} & \mathbf{C}_{ar} \\ -\mathbf{C}^{\mathrm{T}}_{ar} & \mathbf{C}_{rr} \end{bmatrix} \begin{bmatrix} \boldsymbol{\epsilon}_a \\ \mathbf{p}_r \end{bmatrix} \tag{9}
$$

with

$$
\begin{aligned}
&\mathbf{p}_a = \begin{bmatrix} N_{xx} & M_{xx} & M_{xs} & N_{xn} \end{bmatrix}^{\mathrm{T}} \\
&\mathbf{p}_r = \begin{bmatrix} N_{xs} & M_{ss} & N_{ss} & N_{sn} \end{bmatrix}^{\mathrm{T}} \\
&\boldsymbol{\epsilon}_a = \begin{bmatrix} \epsilon^0_{xx} & \kappa_{xx} & \kappa_{xs} & \gamma_{xn} \end{bmatrix}^{\mathrm{T}} \\
&\boldsymbol{\epsilon}_r = \begin{bmatrix} \gamma^0_{xs} & \kappa_{ss} & \epsilon^0_{ss} & \gamma_{sn} \end{bmatrix}^{\mathrm{T}}
\end{aligned} \tag{10}
$$

where the subscripts a and r denote the active and reactive components, respectively.

3.3. Governing equations

The governing equations for the shell wall of the section are derived using a mixed variational theorem by Reissner (Ref. 28-29) which states

$$
\delta\Pi = \delta U - \delta W = 0 \tag{11}
$$

where δU is the virtual strain energy per unit length and δW is the external virtual work done over the cross-sectional area A per unit length, respectively given as:

$$
\delta U = \int_C \left[\underline{\delta\boldsymbol{\epsilon}_a^{\mathrm{T}} \mathbf{p}_a + \delta\left(\boldsymbol{\epsilon}_r^k\right)^{\mathrm{T}} \mathbf{p}_r} + \delta\mathbf{p}_r^{\mathrm{T}} \left(\boldsymbol{\epsilon}_r^k - \boldsymbol{\epsilon}_r\right) \right] ds \tag{12}
$$

$$
\delta W = \left(\int_A \delta\mathbf{u}_c^{\mathrm{T}} \mathbf{t} dA \right)_{,x} \tag{13}
$$

where C is the length of the sectional contour, $\boldsymbol{\epsilon}_r^k$ is the kinematically defined reactive strains as written in Eq. (1), $\mathbf{t} = \begin{bmatrix} \sigma_{xn} & \sigma_{xs} & \sigma_{xx} \end{bmatrix}^{\mathrm{T}}$ is the surface traction vector over the cross-section area, and $\mathbf{u}_c$ is the displacement vector of an arbitrary material point of the shell wall away from the midplane, respectively. It should be noted that the other pair of the reactive strains ($\boldsymbol{\epsilon}_r$) appeared in Eq. (12) is obtained from the constitutive relations (Eq. (9)). Combining Eqs. (1), (12), and (13), the variational statement of Eq. (11) leads to a set of Euler-Lagrange equations as:

$$
\begin{aligned}
&N_{xs,s} + N_{xx,x} = 0; \quad N_{ss,s} + N_{sn}/a + N_{xs,x} = 0 \\
&N_{sn,s} - N_{ss}/a + N_{xn,x} = 0; \quad M_{xs,s} - N_{xn} + M_{xx,x} = 0 \\
&M_{ss,s} - N_{sn} + M_{xs,x} = 0
\end{aligned} \tag{14}
$$

along with the constraint conditions for the reactive strains and curvature measures respectively written as:

$$
\gamma^k_{xs} = \gamma_{xs}; \quad \kappa^k_{ss} = \kappa_{ss}; \quad \epsilon^k_{ss} = \epsilon_{ss}; \quad \gamma^k_{sn} = \gamma_{sn} \tag{15}
$$

The constraint conditions set for the reactive strains $\boldsymbol{\epsilon}_r$ in Eq. (12) are satisfied in a weak sense, with $\delta\mathbf{p}_r$ acting as the Lagrange multiplier. Using Eq. (14)

while performing the integration by parts along the contour coordinates s results in the reactive stress resultants and couples vector $\mathbf{p}_r = \begin{bmatrix} N_{xs} & M_{ss} & N_{ss} \end{bmatrix}^{\mathrm{T}}$ expressed as (Ref. 15, 27):

(16) $$\mathbf{p}_r = \mathbf{B}_p \mathbf{p}_r^0 - \mathbf{p}_r^b$$

with

$$\mathbf{B}_p = \begin{bmatrix} 1 & 0 & 0 & 0 \\ 0 & 1 & z & -y \\ 0 & 0 & y_{,s} & z_{,s} \end{bmatrix}$$

(17) $$\mathbf{p}_r^0 = \begin{bmatrix} N_{xs}^0 & M_{ss}^0 & N_y^0 & N_z^0 \end{bmatrix}^{\mathrm{T}}$$
$$\mathbf{p}_r^b = \begin{bmatrix} \int_{s_0}^{s} N_{xx,x} ds & \int_{s_0}^{s} \left(2M_{xs,x} + N_{xs,x} r_n \right) ds & N_{xs,x} r_t \end{bmatrix}^{\mathrm{T}}$$

where $\mathbf{p}_r^0$ contains the unknown constants of integration defined for each cell of a closed cross-sectional profile and $\mathbf{p}_r^b$ corresponds to branch reactive stress resultants which vary along the contour. Inserting Eq. (16) into the constraint terms $\delta \mathbf{p}_r^{\mathrm{T}}$ of Eq. (12) yields the continuity conditions on the reactive strains that must be satisfied for the closed section:

(18) $$\oint \mathbf{B}_p^{\mathrm{T}} \boldsymbol{\epsilon}_r ds = \mathbf{A}_s \mathbf{q}_e + \mathbf{a}_\omega$$

with $\mathbf{A}_s$ and $\mathbf{a}_\omega$ written as

(19)

$$\mathbf{A}_s = \begin{bmatrix} 0 & \oint r_n ds & 0 & 0 \\ 0 & 0 & 0 & 0 \\ 0 & 0 & 0 & 0 \\ 0 & 0 & 0 & 0 \end{bmatrix}, \quad \mathbf{a}_\omega = \begin{bmatrix} \oint \left(\omega_{y,x} y_{,s} + \omega_{z,x} z_{,s} \right) ds \\ 0 \\ 0 \\ 0 \end{bmatrix}$$

where the symbol $\oint$ denotes a closed-loop integral over the contour of the cross-section. It is remarked that there exist four sets of constraint equations for each cell of closed, multi-cell sections. Using Eqs. (5), (9), and (16), Eq. (18) can be expanded further to yield:

(20) $$\left(\oint \mathbf{B}_p^{\mathrm{T}} \mathbf{C}_{rr} \mathbf{B}_p ds \right) \mathbf{p}_r^0 = \underline{\left(\oint \mathbf{B}_p^{\mathrm{T}} \mathbf{C}_{ar}^{\mathrm{T}} \mathbf{B}_q ds + \mathbf{A}_s \right) \mathbf{q}_e} \\ \underline{\underline{+ \oint \mathbf{B}_p^{\mathrm{T}} \boldsymbol{\epsilon}_{ax} ds + \oint \mathbf{B}_p^{\mathrm{T}} \mathbf{C}_{rr} \mathbf{p}_r^b ds + \mathbf{a}_\omega}}$$

Treating the underscored terms in Eq. (20) requires special caution and this is elaborated in the next subsection.

3.4. Reactive stress resultants and warping functions

The unknown constants $\mathbf{p}_r^0$ in Eq. (20) and the warping functions $\boldsymbol{\omega} = \begin{bmatrix} \omega_x & \omega_y & \omega_z & \Psi_s \end{bmatrix}^{\mathrm{T}}$ should be determined to find the force-displacement relations of closed section contours. This is accomplished through progressive steps according to the level of the beam theory desired for the analysis. At first, it is assumed that the beam is under pure extension, torsion and bending (i.e., Euler-Bernoulli beam), which essentially leads to $\mathbf{q}_{e,x} = 0$ (no axial variation). This makes the doubly-underlined terms in Eq. (20) disappear and $\mathbf{p}_r^0$ can be obtained using only the singly-underlined term. This enables to write the reactive stresses $\mathbf{p}_r$ as a function of $\mathbf{q}_e$, thereby making the warping functions expressed also in terms of $\mathbf{q}_e$ through using Eqs. (3), (5), (9) and (16), which are written simply as:

(21) $$\mathbf{p}_r = \mathbf{R}_q \mathbf{q}_e \\ \boldsymbol{\omega} = \boldsymbol{\Omega}_q \mathbf{q}_e$$

where $\mathbf{R}_q$ denote the reactive stresses for a closed cell of the section and $\boldsymbol{\Omega}_q$ represents the warping deformations associated with each entry in $\mathbf{q}_e$, respectively.

Next, we step into the condition that $\mathbf{q}_{e,x} \neq 0$ and $\mathbf{q}_{e,xx} = 0$. This is equivalent to a Timoshenko beam and enables to express $\boldsymbol{\epsilon}_{ax}$, $\mathbf{p}_r^b$ and $\mathbf{a}_\omega$ respectively in terms of $\mathbf{q}_{e,x}$ by using Eqs. (5), (9), (17) and (21). With the updated expression, one can determine the doubly-underlined terms in Eq. (20) and the unknown constants in $\mathbf{p}_r^0$ corresponding to the beam displacement derivatives $\mathbf{q}_{e,x}$. This leads to new $\mathbf{p}_r$ and $\boldsymbol{\omega}$ as functions of $\mathbf{q}_e$ and $\mathbf{q}_{e,x}$ using the same sets of equations (Eqs. (3), (5), (9), (16)) like in the first step as:

(22) $$\mathbf{p}_r = \mathbf{R}_q \mathbf{q}_e + \mathbf{R}_{qx} \mathbf{q}_{e,x} \\ \boldsymbol{\omega} = \boldsymbol{\Omega}_q \mathbf{q}_e + \boldsymbol{\Omega}_{qx} \mathbf{q}_{e,x}$$

where $\mathbf{R}_{qx}$ denote the reactive stresses distributed over the section contour and $\boldsymbol{\Omega}_{qx}$ represent the axial warping deformations associated with each entry in the first derivative of $\mathbf{q}_e$, respectively.

In the final step, both the first and second derivatives of $\mathbf{q}_e$ are retained while the third derivative terms are vanished (i.e., $\mathbf{q}_{e,x} = \mathbf{q}_{e,xx} \neq 0$ and $\mathbf{q}_{e,xxx} = 0$). This takes into account the effects of the restrained torsion due to the boundary constraints at the ends considered in the beam model. The solutions from the second step (Eq. (22)) are used to update ϵ_{ax}, $\mathbf{p}_r^b$, and $\mathbf{a}_\omega$ with the help of Eqs. (5), (9), (17). The unknown constants in $\mathbf{p}_r^0$ corresponding to $\mathbf{q}_{e,xx}$ are then obtained and fed to refine $\mathbf{p}_r$ and $\boldsymbol{\omega}$ as functions of $\mathbf{q}_e$, $\mathbf{q}_{e,x}$ and $\mathbf{q}_{e,xx}$, again using the same sets of equations (Eqs. (3), (5), (9), (16)) like in the previous steps:

(23)
$$\begin{aligned} \mathbf{p}_r &= \mathbf{R}_q \mathbf{q}_e + \mathbf{R}_{qx} \mathbf{q}_{e,x} + \mathbf{R}_{qxx} \mathbf{q}_{e,xx} \\ \boldsymbol{\omega} &= \boldsymbol{\Omega}_q \mathbf{q}_e + \boldsymbol{\Omega}_{qx} \mathbf{q}_{e,x} + \boldsymbol{\Omega}_{qxx} \mathbf{q}_{e,xx} \end{aligned}$$

where $\mathbf{R}_{qxx}$ and $\boldsymbol{\Omega}_{qxx}$ denote the resultant shell loads components and the axial warping functions according to the second derivative of $\mathbf{q}_e$, respectively. Considering only the effect of torsion in $\mathbf{q}_{e,xx}$ (i.e., Vlasov-level beam), this leads to rearrangement of the terms in $\mathbf{p}_r$ and $\boldsymbol{\omega}$ in Eq. (23) which yields the reduced set of equations as:

(24)
$$\begin{aligned} \mathbf{p}_r &= \overline{\mathbf{R}}_q \mathbf{q}_b + \overline{\mathbf{R}}_{qx} \mathbf{q}_{b,x} \\ \boldsymbol{\omega} &= \overline{\boldsymbol{\Omega}}_q \mathbf{q}_b + \overline{\boldsymbol{\Omega}}_{qx} \mathbf{q}_{b,x} \end{aligned}$$

where the overbar denotes the modification into the quantities appeared in Eq. (22). $\mathbf{q}_b = \begin{bmatrix} U_{,x} & \phi_{,x} & \beta_{y,x} & \beta_{z,x} & \phi_{,xx} \end{bmatrix}^{\mathrm{T}}$ denotes the generalized beam strain vector which includes the axial variation in torsion in $\mathbf{q}_e$.

3.5. Cross-sectional constitutive relations

Once the reactive stress resultants and the warpings are determined, one can find the force-displacement relations of the beam cross-section. Combining Eqs. (5), (9) and (24), the singly-underlined parts in the strain energy expression in Eq. (12) leads to the cross-sectional stress resultants $\mathbf{F}_b = \begin{bmatrix} F_x & M_x & M_y & M_z & M_\omega \end{bmatrix}^{\mathrm{T}}$ expressed in terms of the generalized beam strains and their derivatives as:

(25)
$$\mathbf{F}_b = \mathbf{K}_{bb} \mathbf{q}_b + \mathbf{K}_{bx} \mathbf{q}_{b,x}$$

where $\mathbf{K}_{bb}$ is a (5×5) cross-sectional stiffness matrix that represents the beam in the Euler-Bernoulli-Vlasov level, and $\mathbf{K}_{bx}$ represents the coupling between $\mathbf{F}_b$ and $\mathbf{q}_{b,x}$. The relationships between $\mathbf{q}_b$ and the transverse shear forces $\mathbf{F}_s$ are yet to be determined. The transverse shear forces affect $\mathbf{F}_b$, resulting in the variations of the shell stress resultants and generalized strains with respect to x. The relations can be derived under a pure shear condition (Ref. 27). Neglecting the higher-order contributions (i.e., $\mathbf{q}_{b,xx}$), the partial differentiation of Eq. (25) by x reduces to:

(26)
$$\mathbf{F}_{b,x} = \mathbf{K}_{bb} \mathbf{q}_{b,x}$$

Considering the equilibrium of forces and moments of the beam in the transverse directions, one can relate the derivative of the sectional stress resultants $\mathbf{F}_{b,x}$ with the transverse shear forces $\mathbf{F}_s$ as:

(27)
$$\mathbf{F}_{b,x} = \begin{bmatrix} 0 & 0 & 0 \\ 0 & 0 & 0 \\ 0 & 1 & 0 \\ -1 & 0 & 0 \\ 0 & 0 & -1 \end{bmatrix} \begin{bmatrix} F_y \\ F_z \\ T_\omega \end{bmatrix} = \mathbf{T}_v \mathbf{F}_s$$

where F_y and F_z are the shear forces in y and z directions and T_ω ($T_\omega = -M_{\omega,x}$) is the warping torque (Ref. 31), respectively. In the derivation of the above relations, the reference origin is adjusted to the sectional shear center whose location from the beam axis origin is determined using the Trefftz condition (Ref. 32) through decoupling of the bending and torsion. It is noted that only the transverse shear forces retain as the independent variables since the Vlasov torsion T_ω is combined with the St. Venant torsion T_{SV} to form a complete torsion equation: $M_x = T_{SV} + T_\omega$ (Ref. 31). Equating Eqs. (26) and (27) yields the relation between $\mathbf{q}_{b,x}$ and $\mathbf{F}_s$. Insertion of this relation into Eq. (25) leads to:

(28)
$$\mathbf{F}_b = \mathbf{K}_{bb} \mathbf{q}_b + \mathbf{K}_{bv} \mathbf{F}_s$$

where $\mathbf{K}_{bv} = \mathbf{K}_{bx} \mathbf{S}_{bb} \mathbf{T}_v$ with the definition of $\mathbf{S}_{bb} = \mathbf{K}_{bb}^{-1}$. A pure shear condition ($\mathbf{F}_b = 0$ and $\mathbf{F}_s \neq 0$) is introduced to relate the generalized beam strains $\mathbf{q}_b$ with the transverse shear forces $\mathbf{F}_s$ as:

$$\mathbf{q}_b = -\mathbf{S}_{bb}\mathbf{K}_{bv}\mathbf{F}_s = \mathbf{S}_{bv}\mathbf{F}_s \tag{29}$$

where we use the notation $\mathbf{S}_{bv} = -\mathbf{S}_{bb}\mathbf{K}_{bv}$. The bending and shear contributions from Eqs. (28) and (29) (under a pure shear condition) are superposed to construct the generalized beam strains $\mathbf{q}_b$ expressed as functions of the generalized beam forces as:

$$\mathbf{q}_b = \mathbf{S}_{bb}\mathbf{F}_b + \mathbf{S}_{bv}\mathbf{F}_s \tag{30}$$

Eq. (30) and $\mathbf{F}_s$ can be written together in matrix form as

$$\begin{bmatrix} \mathbf{q}_b \\ \mathbf{F}_s \end{bmatrix} = \begin{bmatrix} \mathbf{S}_{bb} & \mathbf{S}_{bv} \\ \mathbf{0} & \mathbf{I}_{2\times 2} \end{bmatrix} \begin{bmatrix} \mathbf{F}_b \\ \mathbf{F}_s \end{bmatrix} \tag{31}$$

where $\mathbf{I}_{2\times 2}$ is a (2×2) identity matrix. The beam cross-sectional stiffness constants considering the effects of the transverse shear, sectional warping, and warping inhibition can now be determined. Inserting Eqs. (5), (9), (24) and (31) into Eq. (12), one obtains the variation of the strain energy in symbolic form as:

$$\delta U = \delta \begin{bmatrix} \mathbf{F}_b \\ \mathbf{F}_s \end{bmatrix}^{\mathrm{T}} \bar{\mathbf{S}}_{7\times 7} \begin{bmatrix} \mathbf{F}_b \\ \mathbf{F}_s \end{bmatrix} \tag{32}$$

where $\bar{\mathbf{S}}_{7\times 7}$ is a (7×7) flexibility matrix which is of the following form:

$$\bar{\mathbf{S}}_{7\times 7} = \int_C \begin{bmatrix} \mathbf{S}_{bb} & \mathbf{S}_{bv} \\ \mathbf{0} & \mathbf{I}_{2\times 2} \end{bmatrix}^{\mathrm{T}} \begin{bmatrix} \mathbf{K}_{bb} & \mathbf{K}_{bv} \\ \mathbf{K}_{bv}^{\mathrm{T}} & \mathbf{K}_{vv} \end{bmatrix} \begin{bmatrix} \mathbf{S}_{bb} & \mathbf{S}_{bv} \\ \mathbf{0} & \mathbf{I}_{2\times 2} \end{bmatrix} ds \tag{33}$$

An inversion of the flexibility matrix yields the (7×7) stiffness matrix: $\bar{\mathbf{K}}_{7\times 7} = \bar{\mathbf{S}}_{7\times 7}^{-1}$. The elements in $\bar{\mathbf{K}}_{7\times 7}$ are properly rearranged so that the force-displacement relations of the beam cross-section are expressed as:

$$\mathbf{F} = \mathbf{K}_{7\times 7}\mathbf{q} \tag{34}$$

where the cross-sectional stress resultant $\mathbf{F}$ and the generalized beam strains $\mathbf{q}$ are respectively defined as:

$$\begin{aligned} \mathbf{F} &= \begin{bmatrix} F_x & F_y & F_z & M_x & M_y & M_z & M_\omega \end{bmatrix}^{\mathrm{T}} \\ \mathbf{q} &= \begin{bmatrix} U_{,x} & \gamma_{xy} & \gamma_{xz} & \phi_{,x} & \beta_{y,x} & \beta_{z,x} & \phi_{,xx} \end{bmatrix}^{\mathrm{T}} \end{aligned} \tag{35}$$

The (7×7) stiffness coefficients describe the beam in a Timoshenko-Vlasov level while incorporating the effects of elastic couplings. Note that the transverse shear couplings essentially influence the (5×5) elements of $\mathbf{K}_{bb}$ so that the stiffness constants $\mathbf{K}_{7\times 7}$ associated with the extension, bending, torsion, and their coupled elements become substantially modified.

3.6. Recovery relations

The stresses (and strains) over the shell wall thickness can be recovered through an inverse-procedure of obtaining the stiffness matrix $\mathbf{K}_{7\times 7}$. Once the 7×7 stiffness constants are determined, the cross-sectional stress resultants $\mathbf{F}$ are used to find $\mathbf{q}_b$ using Eq. (30). $\mathbf{q}_b$ and $\mathbf{F}_s$ are then used to evaluate the sectional warpings and the reactive stress resultants as given by Eq. (24), which in turn gives the active strains of Eq. (5). The reactive strains ϵ_r can also be recovered from Eq. (9). The recovered strains and curvatures at the midplane are then used to calculate the layer-wise off-axis strains $\boldsymbol{\epsilon}_{\mathrm{off}} = \begin{bmatrix} \epsilon_{xx} & \epsilon_{ss} & \gamma_{xs} \end{bmatrix}^{\mathrm{T}}$ at an arbitrary location of the shell wall, with an offset n along the thickness direction as: $\boldsymbol{\epsilon}_{\mathrm{off}} = \boldsymbol{\epsilon}^0 + n\boldsymbol{\kappa}$. Finally, the off-axis stresses $\boldsymbol{\sigma}_{\mathrm{off}} = \begin{bmatrix} \sigma_{xx} & \sigma_{ss} & \sigma_{xs} \end{bmatrix}^{\mathrm{T}}$ are evaluated using the stress-strain relations $\boldsymbol{\sigma}_{\mathrm{off}} = \bar{\mathbf{Q}}\boldsymbol{\epsilon}_{\mathrm{off}}$ where $\bar{\mathbf{Q}}$ denotes the off-axis lamina stiffness matrix (Ref. 30).

It should be mentioned that the overall procedure to obtain the field variables (e.g., stresses and strains) are purely analytical, in the sense that all the cross-sectional stiffness constants and sectional warpings are obtained by analytical integrations, which does not require interior domain descretizations, heavy numerical factorizations, and/or eigenvalue analyses throughout the entire solution stage.

4. NUMERICAL EXAMPLES

Numerical simulations are performed to demonstrate the validity of the proposed methodology. The examples cover thin-walled beams with highly heterogeneous section, 8-layered rectangular solid section, single-cell box section with circumferentially uniform

Table 1. Comparison of section constants for highly heterogeneous section.

Properties	Analytical	PreComp (Ref. 18) (%)[a]	VABS (Ref. 18) (%)[a]	Present (%)[a]
K_{11} ×10^7 (N)	1.906	2.002 (5.06)	1.905 (-0.06)	1.906 (0.00)
K_{13} ×10^5 (N-m)	1.053	-0.319 (-130.26)	1.042 (-1.04)	1.043 (-0.93)
K_{14} ×10^5 (N-m)	-2.191	2.464 (-212.46)	-2.176 (-0.68)	-2.194 (0.15)
K_{22} ×10 (N-m^2)	4.918	0.000 (-100.00)	4.952 (0.69)	4.951 (0.67)
K_{33} ×10^3 (N-m^2)	2.463	1.652 (-32.93)	2.463 (0.00)	2.454 (-0.36)
K_{34} ×10^2 (N-m^2)	-6.263	-13.850 (121.14)	-6.132 (-2.09)	-6.236 (-0.43)
K_{44} ×10^3 (N-m^2)	3.542	15.430 (335.63)	3.510 (-0.90)	3.546 (0.12)
y_{sc} ×10^{-3} (m)	-4.548	11.000 (-341.86)	-4.472 (-1.67)	-4.554 (0.13)
z_{sc} ×10^{-3} (m)	-8.004	-4.000 (-50.02)	-7.981 (-0.29)	-7.983 (-0.27)

[a]Percentage differences are evaluated with respect to the analytical solution as: (Analysis – Analytical)/Analytical×100.

stiffness (CUS) layup, and multi-celled wind turbine blade with elastic couplings.

4.1. Highly heterogeneous section

The first example is a highly heterogeneous section beam that has been studied in Ref. 33. The cross-sectional configuration with geometric dimensions is depicted in Fig. 2. The cross-section is essentially an open channel section made out of the real material while a fake material region is additionally placed to make the section closed. This kind of section arrangements is useful to confirm the validity of any cross-section analysis codes for the application of either open or closed cross-section beams. The material properties of the real material are: Young's modulus E = 206.843 GPa, Poisson's ratio ν = 0.33 and density ρ = 1068.69 kg/m^3. The material properties of the fake material are the same as the real material except the Young's modulus and density being 1.0×10^{-12} times smaller than the real material (Ref. 33).

Table 1 compares the present stiffness results and shear center locations with those obtained from other analysis methods cited in Ref. 33. The stiffness constants K_{ij}'s are the entries located at i-th row and j-th column of the matrix $\mathbf{K}_{bb}$. y_{sc} and z_{sc} are the y and z coordinates of the shear center measured from the sectional reference origin (Fig. 2). The present theory computes the sectional properties considering the section as open or closed, and no differences in the properties appear to be found between them. It is observed that the present predictions show excellent agreements with the analytical solution and other FE-based approaches except PreComp (Ref. 33). The maximum discrepancy is less than 1% as compared with the analytical solution obtained in Ref. 33.

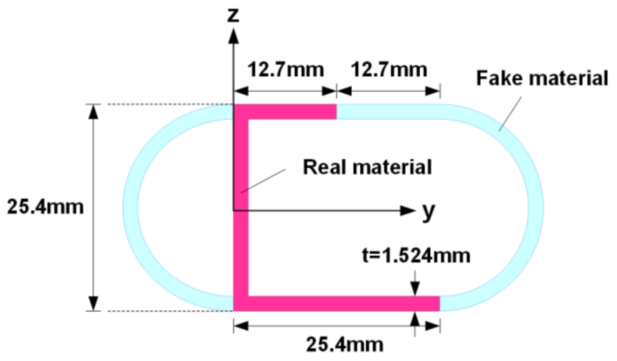

Figure 2. Schematic of highly heterogeneous section.

For both stiffness constants and shear center locations, the present predictions indicate excellent agreements with the analytic solutions. This assures the quality and validity of applying the present beam analysis for open closed section contours. It is noted that the material considered is of isotropic and the coupling (e.g., extension-bending) is induced by the geometric asymmetry of the section.

4.2. 8-layer laminated beam

The next example is an anisotropic strip section beam. The geometry and material distribution of the beam is presented in Fig. 3. The beam is composed of orthotropic layers with a cross-ply symmetric layup [(0/90)$_2$]$_s$. The material properties used are: E_1 = 110.5 GPa, E_2 = E_3 = 13.64 GPa, G_{12} = G_{13} = G_{23} = 3.26 GPa, ν_{12} = ν_{13} = 0.329, ν_{23} = 0.4 (Ref. 34). The root of the beam is clamped with the other end loaded by concentrated forces of F_x = 10 kN and F_z = -10 kN. The beam has been analyzed by Liu and Yu (Ref. 34) in which a 2D FE cross-sectional analysis combined with 1D beam model is used. It is noted that the present approach evaluates the section properties purely on an analytical basis so that the beam stiffness coefficients can be expressed in

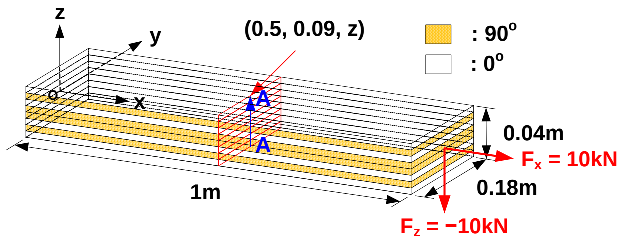

Figure 3. Schematic of 8-layer laminated beam.

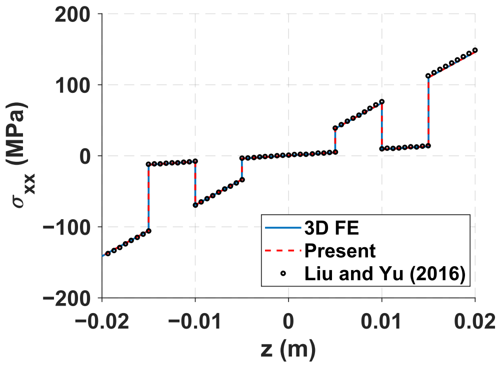

(a) Axial normal stress

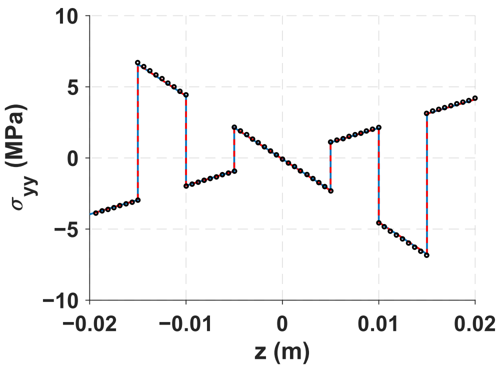

(b) Transverse normal stress

Figure 4. Comparison of predicted normal stresses through the thickness.

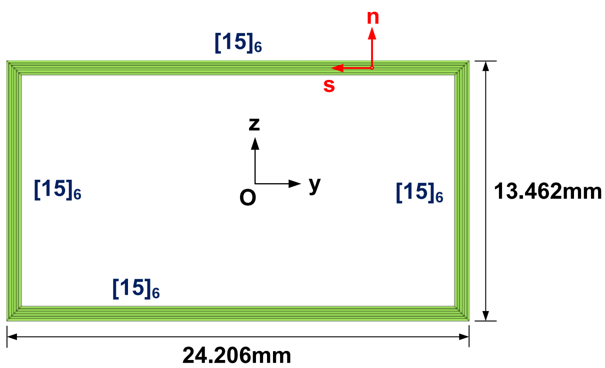

Figure 5. Schematic of composite single-cell box section.

explicit form as the natural outcome the derivation.

In Figure 4, the present predictions on the stresses of the 8-layered beam are correlated with the numerical results of Liu and Yu (Ref. 34) and a 3D FE model. The 3D FE model is created using 57,600 20-noded hexahedral (CHEXA) elements and analyzed using MSC.NASTRAN (https://hexagon.com/products/product-groups/computer-aided-engineering-software/msc-nastran). A RBE2 element is included at the loading end to apply the external forces. Figure 4 compares the layer-wise distributions of the axial and transverse normal stresses across the thickness of the section (A-A line in Fig. 3), respectively. As can be seen, the present predictions on sectional stresses show excellent agreements with those of the detailed 3D solid FE and 2D section analyses with significantly less computational costs (0.3s vs 485s). This close agreement assures again the prediction capability of the proposed composite beam analysis for simple geometry of uncoupled configurations.

4.3. Single-cell composite box section

The next example is an elastically coupled, single-cell composite box section (Ref. 35) as shown in Fig. 5. The positive ply orientation angle is defined as the right-hand rule about the local n axis. The section has circumferentially uniform stiffness (CUS) layup which exhibits extension-torsion and bending-shear couplings. The material properties used are found in Ref. 35 as: E_1 = 141.96 GPa, E_2 = E_3 = 9.79 GPa, G_{12} = G_{13} = 6.00 GPa, G_{23} = 4.80 GPa, ν_{12} = ν_{13} = 0.3, ν_{23} = 0.34. The effective length of the beam is 762 mm (Ref. 36).

Table 2 compares the non-zero stiffness constants predicted for the CUS box section. Only the Timoshenko-level stiffnesses are considered for fair comparison between the results. The cited results are obtained using 2D FE-based section analysis methods. NABSA (Ref. 6) and VABS (Ref. 35) are displacement-based, generic section analysis codes, respectively. Jung et al. (Ref. 15) shares the same theoretical basis with the present theory with additional assumptions including of zero hoop normal stress flow along wall contours (N_{ss}=0) and no in-plane sectional deformation. Reasonable correlations are observed for all the stiffness constants with maximum difference of 3.5% in the flapwise shear stiffness (K_{33}) compared to NABSA. The release of the zero-hoop normal stress flow assumption seems

Table 2. Comparison of stiffness constants of single-cell composite box section with CUS layup.

Stiffness	NABSA (Ref. 35)	VABS (Ref. 35) (%)[a]	Jung et al. (Ref. 15) (%)[a]	Present (%)[a]
$K_{11}\times10^{6}$ (N)	6.3965	6.3921 (-0.07)	6.3934 (-0.05)	6.3934 (-0.05)
$K_{14}\times10^{4}$ (N-m)	-1.2146	-1.2135 (-0.09)	-1.2125 (-0.17)	-1.2125 (-0.17)
$K_{22}\times10^{5}$ (N)	4.0114	4.0154 (0.10)	3.9450 (-1.66)	3.9463 (-1.62)
$K_{25}\times10^{3}$ (N-m)	5.8797	5.8763 (-0.06)	5.8707 (-0.15)	5.8726 (-0.12)
$K_{33}\times10^{5}$ (N)	1.749	1.7539 (0.28)	1.6874 (-3.52)	1.6878 (-3.50)
$K_{36}\times10^{3}$ (N-m)	6.369	6.3667 (-0.04)	6.3319 (-0.58)	6.3339 (-0.55)
$K_{44}\times10$ (N-m^2)	4.8155	4.8184 (0.06)	4.7510 (-1.34)	4.7510 (-1.34)
$K_{55}\times10^{2}$ (N-m^2)	1.9004	1.9001 (-0.02)	1.8914 (-0.47)	1.8916 (-0.46)
$K_{66}\times10^{2}$ (N-m^2)	4.9533	4.9504 (-0.06)	4.9425 (-0.22)	4.9434 (-0.20)

[a]Percentage differences are evaluated with respect to NABSA as: (Analysis - NABSA)/NABSA×100.

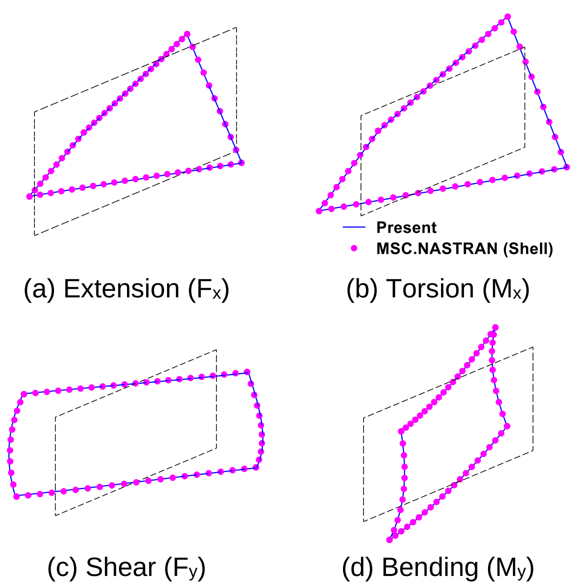

Figure 6. Isometric view of fundamental warping modes under unit sectional loads.

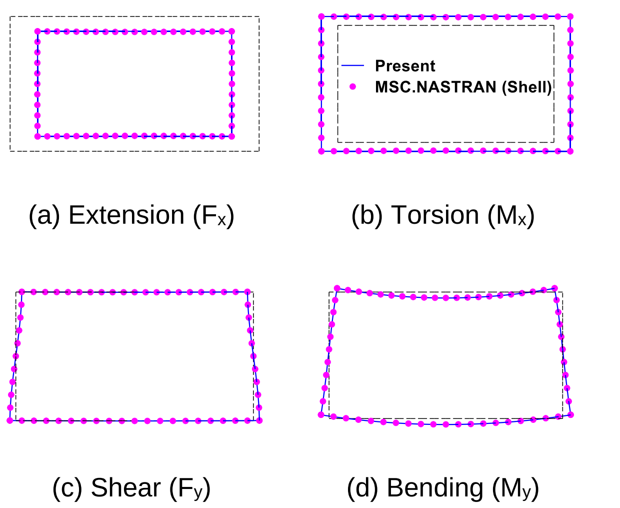

Figure 7. Planar view of fundamental warping modes under unit sectional loads.

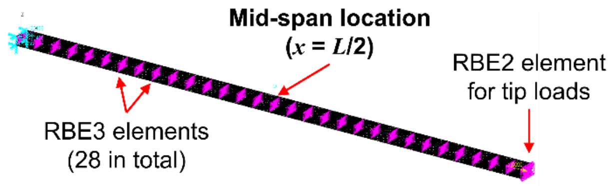

Figure 8. Schematic of shell FE model for single-cell composite box beam.

to make slight improvement on the stiffness constants especially related to bending-shear couplings compared to the results from Jung et al.

Figures 6 and 7 show fundamental warping modes for the CUS box section subjected to unit sectional loads of extension, torsion, chordwise shear, and flapwise bending in isometric and planar views, respectively. Not only the out-of-plane deformations, but also the in-plane warping modes are clearly captured due to Poisson effect. For the validation of the present warping solutions, the results from a shell FE model shown in Fig. 8 are compared with the present solutions. The shell FE model contains 36,000 4-noded quadrilateral elements (CQUAD4) resulting in 216,546 DOFs and was analyzed by MSC.NASTRAN. Like in the previous example, a RBE2 element is defined at the loading end while 28 RBE3 elements are installed in the model to extract the displacements of the beam reference line (U, V, W, ϕ, β_y, β_z). The warping modes of the shell FE model are then computed using Eq. (4). The warping values at the half-span of the beam were extracted to minimize end effects. Due to the elastic couplings, mutual sharing of the warping deformations between different modes are observed. For example, the extension (F_x) mode shares the warping deformations with the torsion (M_x) mode. In the case of the torsion mode, the in-plane deformation tends to make expansion of the cross-section in in-plane

Table 3. Comparison of stiffness constants of a realistic wind turbine blade section.

Stiffness	VABS (Ref. 38)	MSG (Ref. 38) (%)[a]	Present (%)[a]
K_{11} ×10^8 (N)	5.4800	5.6800 (3.59)	5.5177 (0.69)
K_{12} ×10^6 (N-m)	-8.2800	-8.7600 (5.83)	-8.8697 (7.12)
K_{13} ×10^7 (N-m)	1.6000	1.6500 (3.29)	1.5898 (-0.64)
K_{14} ×10^8 (N-m)	-3.8900	-4.0300 (3.73)	-3.8983 (0.21)
K_{22} ×10^6 (N-m^2)	6.0200	6.1200 (1.60)	6.1748 (2.57)
K_{23} ×10^5 (N-m^2)	-3.4500	-3.6000 (4.56)	-3.6293 (5.20)
K_{24} ×10^6 (N-m^2)	4.7300	5.0900 (7.69)	4.9723 (5.12)
K_{33} ×10^6 (N-m^2)	6.4600	6.6800 (3.49)	6.4841 (0.37)
K_{34} ×10^6 (N-m^2)	-9.5800	-9.8900 (3.37)	-9.5509 (-0.30)
K_{44} ×10^6 (N-m^2)	3.6300	3.7800 (4.09)	3.6219 (-0.12)

[a]Percentage differences are evaluated with respect to VABS as: (Analysis - VABS)/VABS×100.

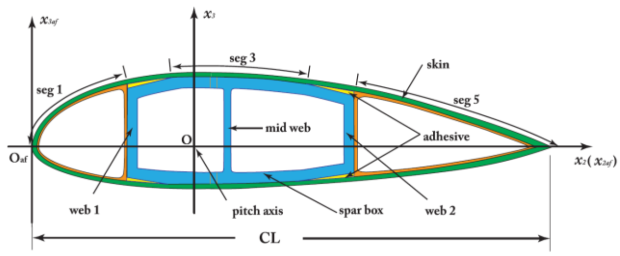

Figure 9. Schematic of a realistic wind turbine blade section (Ref. 37).

direction, which is evidenced by the negative value of K_{14} in Table 2. The chordwise shear mode (F_y) also shares the warping mode with the flapwise bending mode (M_y). Comparing the computation time, the present analysis takes about 0.014 seconds while the shell FE solution needs 113 seconds to get the results, which shows the present analysis makes great reduction in computation time while preserving the solution accuracy.

4.4. Realistic wind turbine blade section

The last example is a realistic wind turbine blade section (Fig. 9) studied in Ref. 37. This section has been employed to examine the analysis capability of the present approach for multi-celled composite blade cross-sections. This section has complex laminate stacking sequences along the wall contours which form unsymmetric sectional shape, thereby yielding a fully-populated stiffness matrix affected from both the material and geometric couplings. The detailed geometric and material properties of the section can be found in Ref. 33. Table 3 compares the stiffness constants obtained between the current analysis and other detailed FE approaches in Ref. 38. The MSG (Mechanics of Structure Genome, Ref. 38) analyzes thin-walled composite beam sections discretized by 1D FE's. The stiffness constants K_{ij} are the entries at the i-th row and the j-th column of the matrix $\mathbf{K}_{bb}$ (Eq. (26)). The present results show good correlations with the other predictions, while indicating better predictions than MSG, for most of the stiffnesses except the torsion-related constants (K_{12}, K_{22}, and K_{23}), as compared with VABS. It is noted that the predicted results from VABS and MSG are obtained respectively using 11,023 2D FE's and 128 1D FE's. However, the present analysis is performed using 16 parametric contours without discretizing the sectional domain, thereby demanding significantly less modeling effort and computational cost.

5. CONCLUDING REMARKS

In this work, a purely analytic beam formulation based on the Reissner's mixed variational theorem has been developed for general thin-walled composite beams with arbitrary geometries and material distributions. Previously adopted zero-hoop assumption was abandoned, with introducing no peculiar or ad hoc assumption to simplify the analysis. All the stresses and sectional warpings (both in- and out-of-plane) were obtained in closed form. The present predictions on sectional warpings, stiffnesses, and stresses were validated against several benchmark examples with different cross-section configurations. The comparison study demonstrated good to excellent agreements with detailed 3D FE analysis and other state-of-the-art beam results. The effects of incorporating the in-plane warpings were shown to be marginal on stiffness coefficients of thin-walled box beams, with some improvements in predictions. The theory implemented into a general-purpose cross-sectional analysis software that could readily be applied for optimum structural designs of composite helicopter or wind turbine blades.

Author contact:

Jae Seong Bae jaiseong@konkuk.ac.kr

Sung Nam Jung snjung@konkuk.ac.kr

6. ACKNOWLEDGMENTS

This work was supported by the National Research Foundation of Korea (NRF) grant funded by the Korean government (MSIT) (2022R1A4A1018884). This work was supported by the National Research Foundation of Korea (NRF) grant funded by the Korean government (MSIT) (2021R1F1A1045570 This work was supported by Korea Research Institute for defense Technology planning and advancement (KRIT) grant funded by the Korea government (DAPA (Defense Acquisition Program Administration)) (No. KRIT-CT-22-082, 2023).

7. REFERENCES

1. Jung, S. N., Nagaraj, V. T., and Chopra, I., "Assessment of Composite Rotor Blade Modeling Techniques," *Journal of the American Helicopter Society*, Vol. 44, 1999, pp. 188-205.

2. Hodges, D. H., *Nonlinear Composite Beam Theory*, American Institute of Aeronautics and Astronautics, Reston, VA, 2006.

3. Hodges, D. H., "Unified Approach for Accurate and Efficient Modeling of Composite Rotor Blade Dynamics," *Journal of the American Helicopter Society*, Vol. 60, 2015, pp. 1-28.

4. Carrera, E., Pagani, A., Petrolo, M., and Zappino, E., "Recent Developments on Refined Theories for Beams with Applications," *Mechanical Engineering Reviews*, Vol. 2, 2015. pp. 14-00298-14-00298.

5. Berdichevskii, V., "On the Energy of an Elastic Rod," *Journal of Applied Mathematics and Mechanics*, Vol. 45, 1981, pp. 518-529.

6. Giavotto, V., Borri, M., Mantegazza, P., Ghiringhelli, G., Caramaschi, V., Maffioli, G., and Mussi, F., "Anisotropic Beam Theory and Applications," *Computers and Structures*, Vol. 16, 1983, pp.403-413.

7. Yu, W., Hodges, D. H., and Ho, J. C., "Variational Asymptotic Beam Sectional Analysis - an Updated Version," *International Journal of Engineering Science*, Vol. 59, 2012, pp. 40-64.

8. Han, S. and Bauchau, O. A., "Nonlinear Three-Dimensional Beam Theory for Flexible Multibody Dynamics," *Multibody System Dynamics*, Vol. 34, 2015, pp. 211-242.

9. Dhadwal, M. K., and Jung, S. N., "Multifield Variational Sectional Analysis for Accurate Stress Computation of Multilayered Composite Beams," *AIAA Journal*, Vol. 57, 2019, pp.1702-1714.

10. Carrera, E., and Giunta, G., "Refined Beam Theories based on a Unified Formulation," *International Journal of Applied Mechanic*s, Vol. 2, 2010, pp. 117-143.

11. Carrrera, E., de Miguel, A., and Pagani, A., "Hierarchical Theories of Structures based on Legendre Polynomial Expansions with Finite Element Applications, *International Journal of Mechanical Sciences*, Vol. 120, 2017, pp. 286-300.

12. Heyliger, P. R., "Elasticity Alternatives to Generalized Vlasov and Timoshenko Models for Composite Beams," *Composite Structures*, Vol. 145, 2016, pp. 80-88.

13. Ho, J. C., "Stiffness Constants of Homogeneous, Anisotropic, Prismatic Beams," *AIAA Journal*, Vol. 53, 2015, pp. 473-478.

14. Smith, E. C., and Chopra, I., "Formulation and Evaluation of an Analytical Model for Composite Box Beams," *Journal of the American Helicopter Society*, Vol. 36, 1991, pp. 23-35.

15. Jung, S. N., Nagaraj, V. T., and Chopra, I., "Refined Structural Model for Thin- and Thick-Walled Composite Rotor Blades," *AIAA Journal*, Vol. 40, 2002, pp. 105-116.

16. Qin., Z., and Librescu, L., "On a Shear-Deformable Theory of Anisotropic Thin-Walled Beams: Further Contribution and Validations," *Composite Structures*, Vol. 56, 2002, pp. 345-358.

17. Vo, T. P., and Lee, J., "Flexural-Torsional Behavior of Thin-Walled Closed-Section Composite Box Beams," *Engineering Structures*, Vol. 29, 2007, pp. 1774-1782.

18. Wang, S., and Zhang, C., "Structure Mechanical Modeling of Thin-Walled Closed-Section Composite Beams, Part 2: Multi-Cell Cross Section," *Composite Structures*, Vol. 113, 2014, pp. 56-62.

19. Saravia, C. M., Gatti, C. D., and Ramirez, J. M., "On the Determination of the Mechanical Properties of Wind Turbine Blades: Geometrical Aspects of Line based Algorithms," *Renewable Energy*, Vol. 105, 2017, pp. 55-65.

20. Vieira, R., Virtuoso, F., and Pereira, E., "A Higher-Order Model for Thin-Walled Structures with

Deformable Cross-Sections," *International Journal of Solids and Structures*, Vol. 51, 2014, pp. 575-598.

21. Han, S., and Bauchau, O. A., "On the Analysis of Thin-Walled Beams based on Hamiltonian Formalism," *Computers and Structures*, Vol. 170, 2016, pp. 37-48.

22. Deo, A., and Yu, W., "Thin-Walled Composite Beam Cross-Sectional Analysis Using the Mechanics of Structural Genome," *Thin-Walled Structures*, Vol. 152, 2020, pp. 106663.

23. Volovoi, V. V., and Hodges, D. H., "Theory of Anisotropic Thin-Walled Beams," *Journal of Applied Mechanics*, Vol. 67, 2000, pp. 453-459.

24. Yu, W., and Hodges, D. H., "Best Strip-Beam Properties Derivable from Classical Lamination Theory," *AIAA Journal*, Vol. 46, 2008, pp. 1719-1724.

25. Harusampath, D., Harish, A. B., and Hodges, D. H., "Model Reduction in Thin-Walled Open-Section Composite Beams Using Variational Asymptotic Method, Part I: Theory," *Thin-Walled Structures*, vol. 117, 2017, pp. 356-366.

26. Reissner, E., and Tsai, W. T., "Pure Bending, Stretching, and Twisting of Anisotropic Cylindrical Shells," *Journal of Applied Mechanics*, Vol. 39, 1972, pp. 148-154.

27. Tsai, W., "On the Problem of Flexure of Anisotropic Cylindrical Shells," *International Journal of Solids and Structures*, Vol. 9, 1973, pp. 1155-1175.

28. Reissner, E., "On Mixed Variational Formulations in Finite Elasticity," *Acta Mechanica*, Vol. 56, 1985, pp. 117-125.

29. Reissner, E., "On Stretching, Bending, Twisting and Flexure of Cylindrical Shells," *International Journal of Solids and Structures*," Vol. 12, 1976, pp. 853-866.

30. Jones, R. M., *Mechanics of Composite Materials*, Taylor and Francis, 1999.

31. Jung, S. N., and Lee, J. Y., "Closed-Form Analysis of Thin-Walled Composite I-Beams Considering Non-Classical Effects," *Composite Structures*, Vol. 60, 2003, pp. 9-17.

32. Pilkey, *Analysis and Design of Elastic Beams: Computational Methods*, John Wiley and Sons, 2002.

33. Chen, H., Yu, W., and Capellaro, M., "A Critical Assessment of Computer Tools for Calculating Composite Wind Turbine Blade Properties," *Wind Energy*, Vol. 13, 2010, pp. 497-516.

34. Liu, X., and Yu, W., "A Novel Approach to Analyze Beam-Like Composite Structures Using Mechanics of Structure Genome," *Advances in Engineering Software*, Vol. 100, 2016, pp. 238-251.

35. Popescu, B., and Hodges, D. H., "On Asymptotically Correct Timoshenko-Like Anisotropic Beam Theory," *International Journal of Solids and Structures*, Vol. 37, 2000, pp. 535-558.

36. Chandra, R., and Chopra, I., "Structural Response of Composite Beams and Blades with Elastic Couplings," *Composites Engineering*, Vol. 2, 1992, pp. 347-374.

37. Deo, A., and Yu, W., "Thin-Walled Composite Beam Cross-Sectional Analysis Using the Mechanics of Structure Genome," Thin-Walled Structures, Vol. 152, 2020, pp. 106663.